# Intercomparison Between *in situ* and AVHRR Polar Pathfinder-derived Surface Albedo over Greenland

Julienne C. Stroeve[1, 2], Jason E. Box[2], Charles Fowler[3], Terence Haran[1], Jeffery Key[4]

[1]National Snow and Ice Data Center, University of Colorado, Boulder
[2]Cooperative Institute for Research in Environmental Sciences, University of Colorado, Boulder
[3]Colorado Center for Astrodynamics Research, University of Colorado, Boulder
[4]Office of Research and Applications, National Environmental Satellite, Data, and Information Service, National Oceanic and Atmospheric Administration, Madison

Address of Correspondence:
Julienne C. Stroeve
National Snow and Ice Data Center (NSIDC)
Cooperative Institute for Research in Environmental Sciences (CIRES)
University of Colorado
Campus Box 449
Boulder, CO 80309-0449
Tel: (303) 492-3584
Fax: (303) 492-2468
Email: stroeve@kodiak.colorado.edu

Accepted to Remote Sensing of the Environment

## Abstract

The Advanced Very High Resolution (AVHRR) Polar Pathfinder Data (APP) provides the first long time series of consistent, calibrated surface albedo and surface temperature data for the polar regions. Validations of these products have consisted of individual studies that analyzed algorithm performance for limited regions and or time periods. This paper reports on comparisons made between the APP-derived surface albedo and that measured at fourteen automatic weather stations (AWS) around the Greenland ice sheet from January 1997 to August 1998. Results show that satellite-derived surface albedo values are on average 10% less than those measured by the AWS stations. However, the station measurements tend to be biased high by about 4% and thus the differences in absolute albedo may be less (e.g. 6%). In regions of the ice sheet where the albedo variability is small, such as the dry snow facies, the APP albedo uncertainty exceeds the natural variability. Further work is needed to improve the absolute accuracy of the APP-derived surface albedo. Even so, the data provide temporally and spatially consistent estimates of the Greenland ice sheet albedo.

## (1) Introduction

Surface albedo, the hemispheric reflectivity integrated over the entire solar spectrum, is a fundamental component for determining the Earth's climate. It is a parameter needed in both global and regional climate models, and for determining surface energy balance. In the polar regions, the high surface albedo acts to cool the lower troposphere and therefore acts as an important boundary condition for energy and heat exchange between the mid-latitudes and the polar regions. The high surface albedo of snow and ice-covered surfaces allows for very little solar energy to be absorbed by the snowpack. However, as the snowpack begins to melt the reduction in surface albedo associated with that melt allows significantly more solar radiation to be absorbed. Consequently, snowmelt comprises an unstable positive feedback component of the climate system, which amplifies small perturbations to that system.

Current estimates of snow albedo fall short of the accuracy needed for climate studies. The accuracy of snow albedo in General Circulation Models (GCMs) is still found to be poor because of inadequate parameterizations (*Roesch et al.*, 1999). Since climatic warming is closely connected with alterations in the surface energy balance and hence, surface albedo, it is essential to monitor these changes in response to changing climatological conditions as accurately as possible.

Although the surface albedo has been routinely observed for some time, maps of surface albedo in the polar regions have not been routinely provided. One of the AVHRR Polar Pathfinder (APP) products are gridded maps of the surface albedo for the polar regions spanning 1981 to 1998 based on observations from the Advanced Very High Resolution Radiometer (AVHRR) on board NOAA POES satellites. This NOAA/NASA Pathfinder program project is currently generating multi-year time series of moderate-resolution products derived primarily from AVHRR data (*Meier et al.*, 1996; *Hutchinson and Scambos*, 1997; *Maslanik et al.*, 1997).

One of the Polar Pathfinder projects' main goals is to provide consistent data sets for the polar regions. The Polar Pathfinder Program helps ensure consistency between current Polar Pathfinder products and provides a transition to similar products derived from existing and forthcoming satellites, such as from the Moderate-Resolution Imaging Spectroradiometer (MODIS). To meet this goal requires validation of the existing Polar Pathfinder Products using field observations.

Validations to date for the APP surface albedo consist of individual studies that analyzed algorithm performance applied to AVHRR data for limited regions and/or time periods (e.g. *Meier et al.*, 1996; *Maslanik et al.*, 1997). While the surface albedo maps over the ice sheets appear qualitatively correct, they are of poorer absolute accuracy than was found in previous studies that examined albedos of sea ice and snow on land.

This paper reports on comparisons made between the 1.25 km AVHRR Polar Pathfinder-derived surface albedo and that measured at fourteen automatic weather stations on the Greenland ice sheet (Figure 1) from 1 January 1997 to 6 August 1998. The main purpose of the study is to validate the existing APP-derived surface albedo estimates, but results of the comparison will also serve to improve AVHRR-derived surface albedo maps for the Greenland ice sheet.

## (2) Data

### 2.1 Satellite Data

The AVHRR Polar Pathfinder data set includes multichannel data and geophysical products derived from AVHRR flown on the NOAA/TIROS operational meteorological satellites (NOAA-7, -9, -11, and -14). The APP product provides continuous daily data from July 1981 through summer 1998, with twice per day surface temperature and albedo and daily sea ice velocities for both polar regions. Considerable effort has been made to provide a consistent data record by cross-calibrating individual instruments and minimizing processing changes over the July 1981 to August 1998 record. The APP products were processed at the Colorado Center for Astrodynamics Research (CCAR) at the University of Colorado and are being archived at the National Snow and Ice Data Center (NSIDC).

The APP data set used in this comparison study is the Version5 1.25–km Polar Pathfinder Product data, derived from the 1-km NOAA-14 AVHRR Level 1b scenes. The Version5 product for the Northern Hemisphere contains 2 Granules per day, near 0400 and 1400 Local Solar Time (LST). Each Granule contains the following products: broadband surface albedo, surface skin temperature, AVHRR channels 1-5, solar zenith angle, relative azimuth angle, satellite elevation angle, cloud mask, orbit mask, ancillary information file and universal time coordinate. The data are gridded onto a Lambert Equal-Area 1.25-km grid derived from SSM/I Pathfinder's EASE Grid (*Armstrong and Brodzik*, 1995). Northern Hemisphere grid coverage extends from the North Pole to 50°N. Data at 1.25-km resolution are currently available from 1993 to 1998.

AVHRR channels 1 and 2 are calibrated using the most recent coefficients developed by the NOAA/NASA AVHRR Pathfinder Calibration Working Group (*Rao and Chen*, 1999). The data are then georeferenced to earth coordinates using an orbital ephemeris model with orbit and clock time corrections (*Baldwin and Emery*, 1995).

APP surface albedo is derived from top-of-the-atmosphere (TOA) AVHRR channel 1 and 2 radiances using several steps as depicted in Figure 2. First, the channel 1 and 2 calibrated TOA reflectances are converted to a broadband reflectance based on a linear relationship between the channel 1 and 2 reflectances and a TOA broadband albedo for snow-covered surfaces. To develop the regression equation, the STREAMER

radiative transfer model (*Key and Schweiger*, 1998) was used to simulate the TOA reflectances over a broad range of viewing and illumination angles and atmospheric conditions (aerosol optical depth and water vapor).

Next, the directionally dependent TOA broadband albedo is converted to a hemispheric albedo using ERBE/GOES-derived anisotropic correction factors (*Suttles et al.*, 1988). The work by *Suttles et al.* (1988) updates earlier work by *Taylor and Stowe* (1984) to convert the directional reflectance to hemispheric albedo. A tri-linear interpolation routine was used to derive the conversion factors as a function of satellite zenith angle, solar zenith angle and relative azimuth angle. Former to this technique, the *Lindsay and Rothrock* (1994) parameterization of the *Taylor and Stowe* (1984) anisotropic correction factors for snow surfaces was used. The two methods are compared later.

Finally, the surface broadband albedo is calculated by correcting for atmospheric extinction after *Koepke* (1989).

Eq. 1

$$\text{Surface albedo} = (\text{TOA broadband albedo} - a) / b$$

The atmospheric correction coefficients 'a' and 'b' were developed from regression of output from the STREAMER radiative transfer model using a variety of atmospheric

conditions and viewing geometries. The atmospheric correction is a function of solar zenith angle, water vapor and aerosol optical depth.

In the atmospheric correction, the aerosol optical depth and ozone concentration are prescribed from climatological averages to be 0.06 and 0.24 cm, respectively. Since no atmospheric profiles of water vapor are available for the Greenland ice sheet, estimates of clear-sky total precipitable water vapor are computed based on differences in temperatures between channels 4 and 5. The conversion from brightness temperature difference to precipitable water vapor was derived from regression of Lowtran-modelled brightness temperatures at 11 and 12 μm and precipitable water obtained from Arctic rawinsonde data. No rawinsonde data from Greenland were used in deriving the conversion.

It is important to note that the APP surface albedo is an "apparent" surface albedo, the ratio of upwelling irradiance to downward irradiance at a specific solar zenith angle and wavelength range. It is the same albedo that is measured by radiometers at the surface and is a function of atmospheric conditions and solar zenith angle.

Cloud screening is applied to the data using algorithms from the Cloud and Surface Parameter (CASPR) toolkit (*Key*, 1999). However, note that the same surface albedo algorithm is performed on all pixels, regardless of cloud cover. Instead of computing a "cloudy" sky albedo, an accompanying cloud mask based on CASPR is

provided with the data to flag pixels labeled as cloudy. The surface albedo for cloud-free pixels has been computed using APP-2 gridded channel reflectances and broadband emissivities developed by *Key et al.* (submitted to JGR). This product is currently part of the MODIS Land Surface Temperature product.

## 2.2 Station Data

Observations of incoming and reflected shortwave radiation (0.4-1.1 μm) are available from The Greenland Climate Network (GC-Net) (*Steffen et al.*, 1996). The GC-Net is part of the Program for Arctic Regional Climate Assessment (PARCA) (Thomas et al. 2000 submitted to JGR May 31 2000) to provide ground truth information for existing and forthcoming satellites in addition to surface energy and mass balance measurements.

There are currently 18 operational GC-Net sites, including the 3 stations installed during the spring of 1999 (see Table 1 and Figure 1). The stations contain instruments to measure the surface radiation balance, turbulent fluxes, conductive heat flux in the snow pack, profiles of temperature, humidity and wind speed and direction, snow height and pressure. Hourly averages are transmitted via a satellite link (GOES or ARGOS) throughout the year. In addition, the measurements are stored locally in solid state memory.

sources of variance. However, the overall difference in the average co-registered albedo was 0.04.

Other errors in the measured surface albedo may result from the following: (1) imperfect or changing instrument level, (2) the instrument 'cosine response' and (3) other problems associated with instrument obstruction by frost or reflections/shadows onto the instrument from the tower. The latter sources of error are infrequent since the instruments are mounted at the end of a boom arm pointed south to minimize shadowing near midnight. However, some problems are still evident in the data, such as rime frost on up-looking pyranometers at the NASA-E site from days 104-117 and at the North Greenland Ice Project (NGRIP) site from days 61-91 during 1998.

The primary source of error in the measurement of surface albedo is instrument level. The bias in the resultant surface albedo may be amplified if either or both LI-CORs are not perfectly level. Such a bias is very difficult to correct. Instrument leveling may drift because of snow compaction effects on tower anchoring, and settling of the boom arm through time, despite the fact that the boom arm has a cable mounted near the tower to provide counter tension. Leveling errors are corrected at each visit (every 1-2 years).

Uncertainties in LI-COR measurements increase at low signal levels, which typically occur at high solar zenith angles. The uncertainty occurs because the

pyranometer response is normalized to a single solar zenith angle, usually 50°. Pyranometer response is less accurate for large solar zenith angles. Departures from highly accurate instruments in excess of 5% are observed for solar zenith angles greater than 75°. For this reason, we limit our quantitative comparisons to solar zenith angles less than 75°.

## (3) Methods

Because the current method for retrieval of surface albedo is valid for clear-sky cases only, accurate cloud detection is critical. The success of cloud detection over snow remains a large source of uncertainty in the current estimates of surface albedo using AVHRR data. Because uncertainties remain in the APP cloud detection method over Greenland, the cloud detection scheme of *Box* (1997) was used instead. This method is based on comparisons between observed incoming solar irradiance with clear-sky irradiance calculations from the FluxNet radiative transfer model (*Key and Schweiger*, 1998), providing an index of effective cloud opacity. The "effective cloud transmission" ($\tau_\varepsilon$) is defined as the ratio of the measured incoming solar radiation to that computed by the radiative transfer model.

Eq. 2

$$T_e = SW_{in,obs}/SW_{in,clr}$$

A $T_e$ value of 1 would imply clear-sky conditions. However, diffuse sky irradiance will act to underestimate true cloud amount. Nonetheless, much effective cloudiness will be captured since clouds often reduce incoming solar radiation.

Comparisons with the PSP have indicated FluxNet computed incoming solar radiation values greater than the measurements by up to 7%. Given the uncertainty of (X) in $T_{eff}$, $T_{eff}$>0.8 is used as a binary indication of clear skies.

## (4) Results

In Figure 3 (a)-(d) the surface albedo at four different AWS sites during the afternoon pass in 1997 are shown. The 4 stations, in order of increasing elevation, are (1) JAR (962m), (2) Swiss Camp (1149m), (3) Crawford Point-CP1 (1958m) and (4) Summit/GISP2 (3150m). These 4 stations represent a transect across the mid-western part of the ice sheet (see Figure 1). The Summit and CP1 stations are in the accumulation facies of the ice sheet. Net annual accumulation at the two sites is 62 cm and 134 cm, respectively. The Swiss Camp is located at the mean equilibrium line altitude of the Greenland ice sheet and thus experiences a zero net annual accumulation. The JAR site is located in the ablation region, and loses approximately 104 cm of snow/ice per year. During 1997, the JAR AWS site was situated in a lake of approximately 500m diameter

that formed during summer. In 1997, the melt pond filled by 67 cm in 94 hours, decreasing the surface albedo from 0.8 when the glacial ice was snow covered, to 0.14 at the time of maximum melt pond depth of ~80 cm in 1997. The AWS tower has since moved upslope of the lake. The JAR AWS is the only station with a net positive energy balance.

Representative surface albedos are shown in Figure 3 for all coincident measurements where both the satellite and *in situ* data were available and where the solar zenith angle was less than 75°. In the Figure we plot the albedo as given by the daily surface albedo data files. Thus, no prior cloud filtering was performed in Figure 3. Although quantitative comparisons can only be made for "clear-sky" cases, these Figures provide a qualitative assessment of how well the APP data represent the general seasonal trends in the surface albedo at the different stations.

The data show that the APP-derived surface albedos produce the same seasonal trends in surface albedo as seen in the station measurements. For example, at the two sites where substantial summer melting occur (e.g. JAR and Swiss Camp) the decrease in albedo associated with that melting is also detected by the satellite surface albedo estimates. At the JAR site, the APP-derived surface albedo tracks the *in situ* albedo well, showing a steady decline in surface albedo as the surface melts and the melt lake fills up with water. On day 176 there is a large drop in the measured surface albedo as the lake

reaches its maximum depth. This albedo reduction is detected by the APP-derived albedo, albeit not as great as seen by the station. One likely reason that the albedo reduction is not as large in the satellite measurement is because of the large satellite footprint size. Thus, the satellite measurement contains information about the surrounding ice in addition to the surface lake. Albedo increases associated with new snowfall events are also detected with the AVHRR measurement, such as on days 215 and 238.

Similarly, at Swiss Camp, albedo variations associated with melt and snow events are detected in the AVHRR measurements. However, during the beginning part of the year in 1997 (March and April) large differences between AVHRR and *in situ* albedos are found. The station measurements show lower than expected surface albedos during March and April, (0.70 to 0.75). The GC-Net measurements suggest a surface that has undergone melting during winter. Occasionally, mid-winter air temperatures exceed the melting point associated with warm air advection in snow and even rain events. There was enough snow accumulation since the previous melt season at this station that the surface should have been indicative of dry snow. However, analysis of the station data suggest that the new snow deposited during March and early April was subsequently blown away, leaving a darker, crusted surface exposed. The surface albedos return to more "normal" values in April 1997 after a 20-cm snowfall that remained at the surface. The reason the satellite detects overall greater surface albedos may be a result of the

differences in footprint sizes between the satellite observation and the ground measurement. Therefore, it's possible that the satellite might be viewing not only places where the new snow has been blown off, but also areas where the snow accumulated.

At higher elevations (~2000m and greater), little summer melting occurs and the *in situ* measured surface albedo does not vary by more than a few percent over the entire season. The APP-albedo exhibits similar stability, except for what appears to be about a 7 to 10-day oscillation in the albedo. This fluctuation in albedo also occurs at the lower elevations, but is more readily detectable at the higher elevation stations where albedos are less variable. The oscillation is believed to be associated with the variation in the satellite elevation angle. For example, in Figure 4 we show the APP-derived surface albedo at the Summit together with the satellite elevation angle at this site. The time period from approximately day 110 to 220 was relatively cloud free, and the *in situ* measurements suggest a relatively constant surface albedo near 0.90. The APP data on the other hand show fluctuations in albedo on the order of 7 to 12% (absolute) that appear to be associated with changes in the satellite viewing angle. Specifically, a large increase in albedo is found when the satellite elevation angle jumps from near 40° (50° off-nadir viewing) to 80-90° (near nadir viewing). This suggests that some angular dependency remain in the APP-derived surface albedo.

In theory, if the conversion is done correctly, there should be no dependence of the hemispheric albedo on satellite viewing angle or relative azimuth angle, provided the scene is stable. One simple way to test the validity of the angular model is to see if the derived albedo changes with viewing angle and relative azimuth angle. In Figure 5 the dependence of the APP-derived surface albedo on relative azimuth angle and satellite elevation angle is shown using two different angular models: (1) Lindsay and Rothrock (1994) and (2) Suttles et al. (1988). In constructing Figure 5, all clear-sky data from the Summit, NGRIP and NASA-U during 1997 were used. These 3 stations were chosen since they are all relatively close to each other and are at high elevations, and thus dependencies that might arise from changing surface conditions (e.g. melt) are minimized. The different symbols in Figure 5 correspond to 3 different relative azimuth angle bins: (*) 0-60°, (+) 60-120°, and (Δ) 120-180°. Discrepancies between the symbols reveal to what extent the angular model is not able to represent the albedo dependence with relative azimuth angle. Results are shown for only one solar zenith angle bin, 60-70°.

To gain a more quantitative measure of the extent to which the two albedos are related we list the clear-sky correlation coefficients computed between the *in situ* and APP-derived surface albedo for all stations during both 1997 and 1998, and for both

passes in Table 2. Results are not presented for stations 4, 10, 11 and 15, where too few overlaps with the satellite data were available and/or there were *in situ* data problems, such as frost on sensors and power outage. Correlation coefficients are listed for clear-sky cases only, cases where $T_{eff} > 0.8$ and where the solar zenith angle is less than 75°. The number of observations used in the regression analysis is given in parenthesis.

In general, the correlation between the two albedos is weak, and at some GC-Net sites no significant correlation exists with the APP albedos. This is especially true during the morning pass, reaffirming that problems in the albedo retrieval are more pronounced at high solar zenith angles. However, this may not be the case since there are less "good" data to work with during the early morning pass because we are limiting the analysis to solar zenith angles less than 75°.

Good agreement, with statistical significance at the 0.0005 level is found at sites where distinct seasonal variations in albedo occur. These are the sites where summer melting occurs; such as at the JAR and Swiss Camp sites. For example, the correlation coefficient is 0.87 at the Swiss Camp in 1998. At this station significant melt occurred in 1998, with 80 cm of snow and 1.4 m of ice melted, resulting in large drops in the surface albedo. Less melt occurred during 1997, and a much lower correlation (0.55) is found. However, the overall lower correlation coefficient is partially a result of differences observed in the early part of the year. Better correlation is found from May through

September, but still less than observed during 1998. Statistical significance (based on students t-test) is also found at Crawford Point-CP1 during the afternoon pass for both years and the morning pass during 1997, and at Crawford Point-CP2 and DYE-2 for the afternoon pass during 1998. These sites also experienced some slight melting during 1997 and 1998. Statistically significant correlation was also found at the TUNU-N site for the afternoon passes in 1997, a site with little change in surface albedo.

Figure 6 illustrates how the correlation between the *in situ* and APP-derived albedo decreases with elevation. The reason for the decrease in correlation is because at the lower elevation sites the smaller-scale albedo fluctuations are masked by the large changes in albedo associated with changes in the snowpack conditions. Thus, there is a high correlation between the albedos at these stations. At the higher elevation sites where little (e.g. Crawford Point) or no (e.g. Summit) melting occurs and the surface albedo variations remain small, the fluctuations in the APP albedo that are not related to changes in snowpack conditions become more significant and the agreement between the two measurements decreases.

Figure 7 compares all available coincident clear-sky *in situ* and APP-derived surface albedo at the stations listed in Table 2, excluding stations 4, 10, 11 and 15. Results show that there is a general negative bias in the APP-derived surface albedos on the order of 10% as compared with the *in situ* measurements. However, if the 4% bias

observed in the LI-COR measurements at the Swiss Camp is applicable over the entire ice sheet, which may or may not be the case, the differences between the *in situ* and satellite measurements would be closer to 6%.

The overall 10% bias is also apparent in the monthly averaged clear-sky surface albedos (Table 3). Again, keeping in mind that the LI-COR albedo are likely biased high, the general differences may be somewhat less. In general, the clear-sky monthly mean *in situ* albedos are greater than the satellite-derived albedos at all the stations and at all times of the year. Exceptions occur during March and April 1997 at the Swiss Camp, the reasons for which were previously discussed; April-June 1998 at NASA-U; and March 1998 at CP2. At NASA-U and CP2 however, these differences are near zero.

Although the two measurements typically differ by 10%, there are times when the differences are nearly zero, such as during 1998 at the NASA-U station. Similarly, differences may greatly exceed 10%, such as during July 1998 at the JAR site, where the clear-sky monthly mean albedos differ by 38%. More variability is observed in the satellite-derived estimates of the clear-sky monthly albedo as noticed by the larger standard deviations in the mean albedo estimates. However, as seen in Figure 8, there doesn't appear to be any clear spatial or seasonal pattern in the magnitude of the differences in albedos or in the variability of the APP mean albedo.

The general seasonal trends in the monthly-averaged clear sky albedos derived from AVHRR agree with the ground-based variations in albedo (e.g. Figure 8). Typically, the albedo is higher in the spring and fall, and lower in the summer as a result of an increase in snow grain size associated with an aging snowpack or snowmelt. At most sites, precipitation occurs in late summer/early fall, and thus the snow albedo is found to be less during summer as the snow pack ages and before accumulation of new snow occurs. At some sites however, such as at Humboldt or the Summit, there is very little change in the surface albedo during summer. At Humboldt for example, the frequency of snowfall and little melting (up-slope advection from the west results in high accumulation at GITS) in this region during summer explains why the summer albedos remain high and change very little.

## (5) Discussion

Comparisons between Greenland AWS station data and the APP-derived surface albedo show that the satellite values are on average about 10% less that the *in situ* measurements. This discrepancy is significant in terms of the amount of energy available for absorption by the surface. For example, an albedo difference of 0.85 to 0.75 can increase the amount of absorbed energy from 15% to 25%. The greater amount of absorbed energy can subsequently impact surface temperatures and ablation. Thus,

accurate parameterization of the snow albedo is important when modeling the surface climate of ice sheets.

Reasons for the differences between the two measurements essentially fall into two different categories: (1) measurement error and (2) algorithm error. Measurement errors affect both the *in situ* and the satellite measurements. Comparison of the LI-COR measured surface albedo with that from the broadband PSP indicates a positive bias of nearly 0.041. This bias partially explains the differences between the ground-based and satellite estimates of the surface albedo. Similarly, calibration of the AVHRR instrument may also lead to errors in the satellite-derived estimates of the surface albedo. Calibration of the AVHRR instrument using the revised post-launch calibration coefficients of *Rao and Chen* (1999) yield albedo values within 5% (relative) to those presented in *Rao and Chen* (1996). Absolute calibration for channel 1 reveals a 3% (relative) accuracy as compared with those by *Rao and Chen* (1999) and *Rao and Chen* (1996). At this time, absolute calibration accuracy for channel 2 is unknown. Furthermore, differences in footprint sizes between the two different observations also contribute to the differences observed between the satellite and *in situ* measurements. The impact of the large satellite footprint size relative to the ground based measurement on the total albedo error is expected to be greatest in regions that experience summer melting and/or lake formation, particularly during melt onset, and least at higher elevations where little change in surface conditions occur.

Errors in the APP algorithm used to derive surface albedo from satellite measurements also may lead to errors in the final surface albedo estimate. It was suggested previously that some albedo error might be caused by the conversion from a directionally dependent reflectance to hemispherical albedo. In the initial processing of the APP surface albedo product, the conversion factors of *Lindsay and Rothrock* (1994) were used. Figure 5 shows that with this angular model, a strong dependency of the albedo with viewing angle remains, particularly for relative azimuths ranging from 0 to 120°. This led to extremely large fluctuations in the surface albedo with satellite viewing angle. With the *Suttles et al.* (1988) model, the model used in the APP processing, the dependence on viewing angle is reduced, although a slight dependence does remain.

Both the *Lindsay and Rothrock* (1994) and *Suttles et al.* (1988) models use the ERBE data. Uncertainties in the ERBE angular correction may lead to an absolute error of nearly 2% in the global mean albedo, but the actual albedo error could be much larger (*Ye*, 1993). Recently, *Li* (1996) showed that problems still remain with the ERBE ADM over snow/ice-covered surfaces, particularly during summer. Further improvements in angular models are expected with the Clouds and the Earth's Radiant Energy System (CERES) instrument. In this paper, we do not attempt to generate a new set of angular models. Owing to the small number of samples used here, we can only provide a qualitative assessment of how well the angular models used in the Polar Pathfinder

processing work over Greenland. However, with the processing of more of the AVHRR data, the possibility will exist to generate a new set of angular models.

Another source of error related to the directional reflectance of snow, is the surface roughness. Recently, *Warren and Brandt* (1998) showed that the angular pattern of sunlight reflected by snow is altered by surface roughness. Roughness in the snow surface causes variations in the incidence angle of the sunlight and may even cause shadowing. These effects were found to greatest at large viewing zenith angles, suggesting that remote sensing of albedo can be carried out accurately without knowledge of surface roughness heights and orientation if near-nadir views are used. In the APP processing, however, derivation of the surface albedo is not limited to near-nadir views, and thus surface roughness is expected to introduce error in the albedo estimates. The magnitude of this error however is unclear. Further work is needed to assess the impact of surface roughness on estimates of snow albedo from satellite.

Other errors in the APP-derived surface albedo may be caused by the narrow-to-broadband conversion. The albedo at the TOA is defined as the fraction of incoming solar irradiance reflected back to space from the earth's surface and the atmosphere. Thus, it is intrinsically dependent upon atmospheric conditions. In the conversion from the two narrowband satellite measurements to a broadband albedo, a linear relationship is used. However, the conversion factors that linearly relate the two narrowband

measurements to the broadband albedo are dependent upon atmospheric conditions. This dependence is shown in Figure 9. Aerosol and ozone optical depths affect the conversion factor for AVHRR channel 1, and atmospheric water vapor affects the conversion factor for AVHRR channel 2. Dependence on solar zenith angle is apparent in both channels. Since the conversion from narrow-to-broadband albedo does depend on atmospheric conditions and atmospheric path length, a broadband albedo derived under a specific atmospheric condition would not necessarily be valid under different atmospheric conditions. The error however is predicted to be small at low solar zenith angles (~0.05 absolute error in albedo for $\theta_o \leq 65°$) and large at high solar zenith angles (~0.15 at $\theta_o = 80°$).

Finally, errors may also result in the atmospheric correction. In the atmospheric correction, all corrections are made assuming the surface is at sea level. As mentioned earlier, the atmospheric correction is performed assuming a constant aerosol optical depth of 0.06 and constant ozone amount of 0.24 cm at all elevations and at all times of the year. Since the atmospheric correction is performed assuming all surfaces at sea level, this method would bias the surface albedos high at the higher elevations. Running a simple test using the 6S radiative transfer model (*Tanre et al.*, 1992) for a broadband top-of-the-atmosphere albedo value of 0.8, and using the same values for column amount of atmospheric ozone, water vapor and aerosols, we find that there would be a 6% difference in the model-derived surface albedo between sea level (0.97) and the summit

(0.91). Most of this difference however is caused by atmospheric water vapor. The atmospheric water vapor derived from the AVHRR brightness temperatures at 11 and 12 μm results in greater column amounts at lower elevations than at the higher elevations (Figure 10). In this regard, elevational affects are somewhat taken into account. The computed precipitable water vapor is also found to vary seasonally, with higher amounts during summer, so that there is a slight seasonal dependence of the atmospheric constituents accounted for in the atmospheric correction.

Finally, the possibility exists that some residual cloud effects might be present. Conditions are assumed clear based on the approach by *Box* (1997). It is possible that thin cirrus or diamond dust are not detected with this method. This would affect the instantaneous observations, but would have a much smaller effect on the overall mean bias reported here.

## (6) Conclusions

The surface energy balance of the polar ice sheets is mainly dependent upon the radiative fluxes, and during daylight periods, it is primarily dependent on the surface albedo. The surface albedo controls the amount of solar energy available for absorption by the snowpack and is thus closely linked with surface melt. Since small changes in the

surface albedo can substantially alter the amount of solar energy absorbed by the surface, accurate parameterization of the surface albedo is essential.

With the completion of the AVHRR Polar Pathfinder Project, we now have gridded maps of the surface albedo for the Arctic and Antarctic spanning the past 18 years. Thus, data are now available to support studies of high-latitude climate-change processes, such as trying to gain a better understanding the complex relationships between melt and accumulation, the energy balance and atmospheric flow patterns. This paper examined the accuracy of the APP surface albedo product over Greenland. Results show that the APP-derived surface albedo tends to be on average about 10% less than the *in situ* measurements, but may be reduced to something on the order of 6% considering that the ground-based measurements are biased high. The differences between the two measurements do not appear to have any spatial or temporal pattern.

Comparisons with ground-based measurements reveal better agreement between the two measurements at sites that have a large range in albedo, sites where seasonal changes in surface conditions occur. At the higher elevation sites where the surface albedo remains relatively constant, the measurement uncertainty exceeds the natural variability. This is a result of combined uncertainties in the calibration, atmospheric conditions, and the various aspects of the retrieval algorithm. The use of an improved angular model to convert the directional reflectance measurement to hemispherical

albedo would likely improve the consistency of the albedo measurements. Data from multiangle observations, such as from the Multiangle Imaging SpectroRadiometer (MISR) or from the Polarization and Directionality of the Earth's Reflectances (POLDER) instruments should lead to improved angular models, as well as improved atmospheric characterization and hence improved albedo accuracy.

Even though the absolute accuracy of the APP-derived surface albedo still falls short of the accuracy required for climate models, the general temporal and spatial changes in surface albedo are reproduced quite well with the satellite estimates. Thus, the present results are useful to GCM modelers because the AVHRR-derived albedos provide better estimates of the albedo than what is available otherwise. In conclusion, the APP-derived surface albedos provide temporally and spatially consistent estimates of the surface albedo over Greenland. Further work may be focused on improving the absolute accuracy of the satellite-derived surface albedo.

*Acknowledgements*

This work was supported under NASA grant #NAG5-6666 and GC-Net NASA Grant #NAGW-4248. AVHRR Polar Pathfinder 5 km Data Set. Digital data available from nsidc@kryos.colorado.edu, Boulder, Colorado, NSIDC Distributed Active Archive Center, University of Colorado at Boulder.

## (7) References

Armstrong, R.L. and M.J. Brodzik, 1995. Earth-gridded SSM/I data set for cryospheric studies and global change monitoring, A1 Symposium of COSPAR Scientific Commission A, Hamburg, Germany, July 11-21, 1994. Proceedings. Satellite monitoring of the earth's surface and atmosphere, Nov. 1995, 115-163.

Baldwin, D., and W.J. Emery, 1995. Spacecraft attitude variations of NOAA-11 inferred from AVHRR imagery, *Int. J. Remote Sens.*, 16, 531-542.

Box, J., 1997. Polar day effective cloud opacity in the Arctic from measured and modeled solar radiation fluxes, M.A. thesis, University of Colorado, Boulder.

Hutchinson, T. and T. Scambos, 1997. High-resolution polar climate parameters derived from 1 km AVHRR data, Proc. 8th. Symp. On Global Change Studies, American Meteorological Society, 284-291.

Key, J., X. Wang, J. Stroeve and C. Fowler, Estimating the cloudy sky albedo of sea ice and snow from space, *J. Geophys. Res.*, submitted.

Key, J., 1999. The Cloud and Surface Parameter Retrieval (CASPR) System for Polar AVHRR User's Guide, Cooperative Institute for Meteorological Satellite Studies, University of Wisconsin, 1227 West Dayton, St., Madison, 59 pp.

Key, J. and A.J. Schweiger, 1998. Tools for atmospheric radiative transfer: Streamer and FluxNet, *Computers & Geosciences*, **24(5)**, 443-451.

Koepke, P., 1989. Removal of atmospheric effects from AVHRR albedos, *J. Appl. Meteorol.*, **28**, 1341-1348.

Li, Z., 1996. On the angular correction of satellite radiation measurements: The performance of ERBE angular dependence model in the Arctic, *Theor. Appl. Climatol.*, **54**, 235-248.

Lindsay, R.W. and D.A. Rothrock, 1994. Arctic sea ice albedo from AVHRR, *J. Climate*, 7, 1737-1749.

Maslanik, J., C. Fowler, J. Key, T. Scambos, T. Hutchinson, and W. Emery, 1997. AVHRR-based Polar Pathfinder products for modeling applications, *Annals of Glaciology*, 35, 171-182.

Meier, W., J. A., Maslanik, J. Key, and C. Fowler, 1996. Retrieval of Arctic surface conditions and cloud properties from AVHRR data: A time series for the Beaufort Sea. In 16th International Geoscience and Remote Sensing Symposium (IGARSS), Remote Sensing for a Sustainable Future, 27-31 May 1996, Lincoln, Nebraska, Proceedings Vol. 1, Piscataway, NJ, Institute of Electrical and Electronics Engineers, 73-75.

Ohumura, A. and N. Reeh, 1991. New precipitation and accumulation maps for Greenland, *Journal of Glaciology*, **37**, 140-148.

Rao, C.R.N. and J. Chen, 1999. Revised post-launch calibration of the visible and near-infrared channels of the Advanced Very High Resolution Radiometer (AVHRR) on the NOAA-14 spacecraft, *Int. J. Remote Sensing*, **20**, 3485-3491.

Rao, C.R.N., and Chen, J. (1996), Post-launch calibration of the visible and near-infrared channels of the Advanced Very High Resolution radiometer on the NOAA-7, -9 and –11 spacecraft, *Int. J. Remote Sens.*, **16**, 1931-1942.

Roesch, A., H. Gilgen, M. Wild and Ohmura, A. (1999), Assessment of GCM simulated snow albedo using direct observations, *Climate Dynamics*, **15**, 405-418.

Steffen, K., J. E. Box, and Abdalati, W. (1996), Greenland Climate Network: GC-Net, in Colbeck, S. C. Ed. CRREL 96-27 Special Report on Glaciers, Ice Sheets andVolcanoes, trib. to M. Meier, pp. 98-103.

Stroeve, J., A. Nolin and K. Steffen, 1997. Comparison of AVHRR-derived and *in situ* surface albedo over the Greenland ice sheet, *Remote Sensing Environment*, **62**, 262-276.

Suttles, J.T., R.N. Green, P. Minnis, G.L. Smith, W.F. Staylor, B.A. Wielicki, I.J. Walker, D.F. Young, V.R. Taylor and Stowe, L.L. (1988), Angular radiation models for Earth-Atmosphere system. Volume I-Shortwave radiation, *NASA Reference Publication* 1184, 144 pp.

Tanre, D., Holben, B.N., and Kaufman, Y.J. (1992), Atmospheric correction algorithm for NOAA-AVHRR products: theory and application, *IEEE Trans. Geosci. Remote Sens.*, **30**, 231-250.

Taylor, V.R., and Stowe, L.L. (1984), Atlas of reflectance patterns for uniform earth and cloud surfaces (NIMBUS-7 ERB-61 days), NOAA Technical Report NESDIS 10, U.S. Department of Commerce, 66 pp.

Warren, S.G., and R.E. Brandt (1998), Effect of surface roughness on bidirectional reflectance of Antarctic snow, *J. Geophys. Res.*, **103**(E11), 25,789-25,807.

Ye, Q. (1993), *The space-scale dependence of the observed anisotropy of reflected radiation*, Ph.D. Dissertation, Oregon State University, 159pp.

**Figure Captions**

*Figure 1.* Map of the Greenland ice sheet showing locations of the AWS stations.

*Figure 2.* AVHRR Polar Pathfinder Surface Albedo Processing Steps.

*Figure 3(a)-(d).* Surface albedo for the afternoon satellite pass during 1997 at 4 stations: (a) JAR, (b) Swiss Camp, (c) Crawford Point, and (4) Summit. Data are shown for all coincident ground-based and satellite measurements. No cloud filtering was performed for this Figure.

*Figure 4.* Surface albedo (bold) and satellite elevation angle at the Summit for the afternoon satellite pass during 1997.

*Figure 5(a)-(b).* Dependence of the APP-derived surface albedo on satellite elevation and relative azimuth angle during 1997 for (a) Lindsay and Rothrock (1994) and (b) Suttles et al. (1988) angular models. Results are shown for solar zenith angles ranging from 60-70° and three different azimuth angle bins: 0-60° (star), 60-120° (cross) and 120-180° (triangle).

*Figure 6(a)-(d).* Comparison between APP-derived and *in situ* measured surface albedo for the afternoon satellite pass during 1997 at 4 stations: (a) JAR, (b) Swiss Camp, (c) Crawford Point and (d) Summit. Plotting criteria include solar zenith angles less than 75° and $\tau>0.8$.

*Figure 7.* Comparison between APP-derived and in situ measured surface albedo for all coincident clear-sky ($\tau>0.8$) cases during 1997 and 1998.

*Figure 8(a)-(d).* Monthly-averaged APP and *in situ* surface albedo for the afternoon satellite pass during 1997 at 4 stations: (a) JAR, (b) Swiss Camp, (c) Crawford Point and (d) Summit. Monthly means are computed for all data where the solar zenith angle is less than 75° and where $\tau>0.8$.

*Figure 9(a)-(b).* The fraction of solar radiation within the AVHRR bands 1 (a) and 2 (b) as a function of changes in solar zenith angle and changes in atmospheric conditions.

*Figure 10.* Precipitable water (cm) derived from the AVHRR brightness temperatures at 11 and 12 μm for the afternoon satellite pass during 1997 at 4 stations: (a) JAR, (b) Swiss Camp, (c) Crawford Point and (d) Summit.

Table 1. Station location and elevation for the AWS sites used.

| **Station Name** | **Latitude** (degrees) | **Longitude** (degrees) | **Elevation** (meters) |
|---|---|---|---|
| 01 Swiss Camp | 69.57 | 49.30 | 1149 |
| 02 Crawford Point (CP1) | 69.88 | 46.97 | 1958 |
| 03 NASA-U | 73.83 | 49.50 | 2368 |
| 04 GITS | 77.14 | 61.10 | 1925 |
| 05 Humboldt | 78.53 | 56.83 | 1995 |
| 06 Summit | 72.58 | 38.50 | 3150 |
| 07 TUNU-N | 78.02 | 33.99 | 2113 |
| 08 DYE-2 | 66.48 | 46.28 | 2053 |
| 09 JAR | 69.50 | 49.68 | 962 |
| 10 Saddle | 66.00 | 44.50 | 2460 |
| 11 South Dome | 63.15 | 44.82 | 2850 |
| 12 NASA-E | 75.00 | 30.00 | 2631 |
| 13 Crawford Point (CP2) | 69.91 | 46.85 | 2005 |
| 14 NGRIP | 75.10 | 42.33 | 2918 |
| 15 NASA-SE | 66.48 | 42.50 | 2400 |

Table 2. Greenland Data Format

| Parameter | Units |
|---|---|
| 1. Station Number | (0-15) |
| 2. Year | (e.g. 1995) |
| 3. Julian Decimal Time UTC | (e.g. 172.2917) |
| 4. SW incoming | $W/m^2$ |
| 5. SW reflected | $W/m^2$ |
| 6. Net all-wave radiation | $W/m^2$ |
| 7. Temperature (C1) | °C |
| 8. Temperature (C2) | °C |
| 9. CS-500 T1 | °C |
| 10. CS-500 T2 | °C |
| 11. Relative Humidity (RH1) | % |
| 12. Relative Humidity (RH2) | % |
| 13. Wind Speed (U1) | m/s |
| 14. Wind Speed (U2) | m/s |
| 15. Wind Direction (Udir1) | deg |
| 16. Wind Direction (Udir2) | deg |
| 17. Local Pressure (BMP) | mb |
| 18. Snow height 1 | m |
| 19. Snow Height 2 | m |
| 20. Snow Temp 1 (deepest) | °C |
| 21. Snow Temp 2 | °C |
| 22. Snow Temp 3 | °C |
| 23. Snow Temp 4 | °C |
| 24. Snow Temp 5 | °C |
| 25. Snow Temp 6 | °C |
| 26. Snow Temp 7 | °C |
| 27. Snow Temp 8 | °C |
| 28. Snow Temp 9 | °C |
| 29. Snow Temp 10 (shallowest) | °C |
| 30. Battery Voltage | VDC |
| 31. 2.0 m wind speed estimate from data | m/s |
| 32. 10.0 m wind speed estimate from data | m/s |
| 33. Height of profile 1 | m |
| 34. Height of profile 2 | m |
| 35. Richardson Number (not using potential temperature) | |
| 36. Peak wind speed from U2 when available | m/s |
| 37. Data quality identifier column 1 | |
| 38. Data quality identifier column 2 | |
| 39. Data quality identifier column 3 | |
| 40. Data quality identifier column 4 | |

Table 2. Correlation coefficients between *in situ* and APP-derived surface albedo for clear sky conditions, defined as having effective cloud opacity values ($\tau$) greater than 0.8 and solar zenith angles less than 75°. Only results with at least 10 clear sky observations are listed. The number of observations used in the regression is given in parenthesis.

| Station | 0400 GMT | 1400 GMT | 0400 GMT | 1400 GMT |
|---|---|---|---|---|
| | *1997* | *1997* | *1998* | *1998* |
| 01 Swiss Camp | | 0.55 (115) | | 0.87 (49) |
| 02 Crawford Pt. | 0.39 (29) | 0.35 (94) | 0.49 (27) | 0.57 (64) |
| 03 NASA-U | 0.28 (28) | 0.04 (40) | 0.21 (35) | 0.21 (46) |
| 05 Humboldt | 0.03 (47) | -0.03 (99) | 0.09 (44) | 0.53 (45) |
| 06 GISP2 | 0.25 (30) | 0.20 (103) | | -0.08 (40) |
| 07 TUNU | 0.41 (38) | 0.41 (108) | | 0.40 (21) |
| 08 DYE-2 | | 0.34 (109) | | 0.37 (62) |
| 09 JAR | | 0.75 (80) | | 0.86 (44) |
| 12 NASA-E | 0.05 (19) | 0.26 (90) | | 0.40 (61) |
| 13 CP-2 | 0.37 (16) | 0.21 (77) | | 0.61 (66) |
| 14 NGRIP | | 0.22 (26) | -0.17 (15) | 0.28 (58) |

Table 3. Mean clear-sky monthly averaged surface albedo and standard deviations for the afternoon pass during 1997 and 1998. Monthly means are computed for all "good" measurements where the solar zenith angle is less than 75° and where the effective cloud opacity ($\tau$) is greater than 0.8. Periods of obvious bad *in situ* data, such as due to instrument riming or instrument tilting, are excluded from the averaging. Number of observations used in the averaging is given in parenthesis.

| St. # | Mar 1997 | Apr 1997 | May 1997 | Jun 1997 | Jul 1997 | Aug 1997 | Sep 1997 | Mar 1998 | Apr 1998 | May 1998 | Jun 1998 | Jul 1998 |
|---|---|---|---|---|---|---|---|---|---|---|---|---|
| 01 *in situ* | 0.71± 0.022 (13) | 0.76± 0.035 (23) | 0.78± 0.025 (18) | 0.69± 0.041 (24) | 0.71 ± 0.052 (18) | 0.75 ± 0.011 (14) | 0.86 ± 0.015 (5) | 0.94 ± 0.022 (12) | 0.89 ± 0.025 (16) | 0.82 ± 0.085 (4) | 0.69 ± 0.002 (3) | 0.63 ± 0.047 (15) |
| 01 APP | 0.82± 0. 048 (13) | 0.79± 0.029 (23) | 0.76± 0.031 (18) | 0.65± 0.042 (24) | 0.64 ± 0.075 (18) | 0.67 ± 0.112 (14) | 0.85 ± 0.083 (5) | 0.82 ± 0.125 (12) | 0.79 ± 0.059 (16) | 0.75 ± 0.064 (4) | 0.66 ± 0.018 (3) | 0.58 ± 0.049 (15) |
| 02 *in situ* | 0.92± 0.017 (4) | 0.89± 0.018 (11) | 0.88± 0.020 (24) | 0.86± 0.016 (21) | 0.88 ± 0.030 (14) | 0.87 ± 0.029 (15) | 0.91 ± 0.031 (7) | 0.90 ± 0.035 (16) | 0.87 ± 0.015 (18) | 0.86 ± 0.054 (8) | 0.85 ± 0.032 (6) | 0.83 ± 0.040 (15) |
| 02 APP | 0.82± 0.046 (3) | 0.83± 0.025 (11) | 0.78± 0.028 (24) | 0.76± 0.037 (21) | 0.80 ± 0.041 (14) | 0.80 ± 0.080 (15) | 0.86 ± 0.111 (7) | 0.83 ± 0.071 (16) | 0.80 ± 0.083 (18) | 0.82 ± 0.055 (8) | 0.78 ± 0.043 (6) | 0.75 ± 0.042 (15) |
| 03 *in situ* | | | | 0.84± 0.018 (10) | 0.85 ± 0.017 (16) | 0.86 ± 0.019 (4) | 0.86 ± 0.008 (3) | | 0.86 ± 0.012 (14) | 0.83 ± 0.009 (9) | 0.83 ± 0.017 (3) | 0.84 ± 0.014 (10) |
| 03 APP | | | | 0.80± 0.090 (10) | 0.75 ± 0.080 (16) | 0.78 ± 0.090 (4) | 0.80 ± 0.117 (3) | | 0.87 ± 0.139 (14) | 0.84 ± 0.044 (9) | 0.84 ± 0.050 (3) | 0.83 ± 0.060 (10) |
| 05 *in situ* | | 0.91 ± 0.012 (20) | 0.90 ± 0.007 (26) | 0.88± 0.018 (24) | 0.90 ± 0.014 (21) | 0.89 ± 0.020 (15) | | | 0.90 ± 0.013 (16) | | | 0.86 ± 0.028 (24) |
| 05 APP | | 0.88 ± 0.046 (20) | 0.82 ± 0.051 (25) | 0.80± 0.063 (24) | 0.77 ± 0.036 (19) | 0.75 ± 0.088 (15) | | | 0.77 ± 0.040 (16) | | | 0.78 ± 0.043 (24) |
| 06 *in situ* | | 0.92 ± 0.011 (7) | 0.89 ± 0.010 (25) | 0.88± 0.013 (28) | 0.90 ± 0.010 (18) | 0.91 ± 0.010 (21) | 0.92 ± 0.015 (6) | | | | 0.89 ± 0.008 (15) | 0.89 ± 0.011 (17) |
| 06 APP | | 0.78 ± 0.072 (7) | 0.82 ± 0.037 (24) | 0.81± 0.037 (28) | 0.85 ± 0.073 (18) | 0.80 ± 0.081 (21) | 0.80 ± 0.158 (5) | | | | 0.84 ± 0.043 (15) | 0.84 ± 0.062 (17) |
| 07 *in situ* | | 0.93 ± 0.022 (16) | 0.90 ± 0.010 (25) | 0.89± 0.010 (28) | 0.89 ± 0.015 (19) | 0.90 ± 0.017 (19) | | | 0.93 ± 0.016 (15) | 0.91 ± 0.004 (5) | | |
| 07 APP | | 0.83 ± 0.078 (16) | 0.81 ± 0.025 (25) | 0.79± 0.017 (28) | 0.79 ± 0.070 (19) | 0.81± 0.054 (19) | | | 0.85 ± 0.077 (15) | 0.84 ± 0.016 (5) | | |
| 08 *in situ* | 0.88 ± 0.007 (9) | 0.87 ± 0.011 (15) | 0.86 ± 0.014 (22) | 0.82 ± 0.025 (18) | 0.85 ± 0.031 (11) | 0.84± 0.043 (18) | 0.89 ± 0.012 (7) | 0.87 ± 0.013 (9) | 0.85 ± 0.009 (11) | 0.87 ± 0.024 (10) | 0.85 ± 0.029 (9) | 0.86 ± 0.035 (18) |
| 08 APP | 0.79 ± 0.052 (7) | 0.78 ± 0.059 (15) | 0.76 ± 0.077 (22) | 0.71± 0.033 (18) | 0.75 ± 0.036 (11) | 0.77 ± 0.061 (18) | 0.78 ± 0.112 (7) | 0.79 ± 0.061 (9) | 0.83 ± 0.046 (11) | 0.80 ± 0.023 (10) | 0.76 ± 0.035 (9) | 0.76 ± 0.069 (18) |
| 09 | 0.91 ± | 0.88 ± | 0.83 ± | 0.68± | 0.70 ± | 0.77 ± | 0.88 ± | 0.91 ± | 0.89 ± | 0.81 ± | 0.73 ± | 0.65 ± |

| | | | | | | | | | | | | |
|---|---|---|---|---|---|---|---|---|---|---|---|---|
| *in situ* | 0.043 (5) | 0.028 (15) | 0.049 (21) | 0.095 (21) | 0.086 (9) | 0.189 (5) | 0.015 (4) | 0.032 (7) | 0.034 (14) | 0.086 (4) | 0.019 (5) | 0.074 (12) |
| 09 APP | 0.82 ± 0.051 (4) | 0.77 ± 0.046 (15) | 0.73 ± 0.093 (21) | 0.58± 0.061 (21) | 0.58 ± 0.088 (9) | 0.65 ± 0.106 (5) | 0.73 ± 0.124 (4) | 0.79 ± 0.109 (7) | 0.75 ± 0.122 (14) | 0.71 ± 0.075 (4) | 0.59± 0.069 (5) | 0.42 ± 0.087 (12) |
| 12 *in situ* | | | | 0.92± 0.010 (24) | 0.92 ± 0.011 (14) | 0.93 ± 0.011 (17) | 0.96 ± 0.011 (10) | | | 0.92 ± 0.019 (18) | 0.89 ± 0.009 (23) | 0.91 ± 0.013 (15) |
| 12 APP | | | | 0.81± 0.015 (24) | 0.81 ± 0.026 (14) | 0.82 ± 0.074 (17) | 0.87 ± 0.045 (10) | | | 0.84 ± 0.052 (18) | 0.81 ± 0.033 (23) | 0.81 ± 0.044 (15) |
| 13 *in situ* | | | | 0.87 ± 0.016 (22) | 0.86 ± 0.025 (16) | 0.85 ± 0.034 (13) | 0.89 ± 0.034 (7) | 0.88 ± 0.038 (5) | 0.86 ± 0.015 (18) | 0.85 ± 0.035 (11) | 0.81 ± 0.050 (7) | 0.79 ± 0.050 (22) |
| 13 APP | | | | 0.77 ± 0.058 (22) | 0.81 ± 0.042 (16) | 0.78 ± 0.075 (13) | 0.86 ± 0.113 (7) | 0.89 ± 0.071 (5) | 0.82 ± 0.092 (18) | 0.80 ± 0.060 (11) | 0.78 ± 0.035 (7) | 0.74 ± 0.049 (22) |
| 14 *in situ* | | | | | | 0.84 ± 0.008 (10) | | | 0.80 ± 0.175 (7) | 0.84 ± 0.010 (16) | 0.83 ± 0.017 (15) | 0.84 ± 0.012 (17) |
| 14 APP | | | | | | 0.82 ± 0.046 (10) | | | 0.74 ± 0.110 (7) | 0.84 ± 0.035 (16) | 0.81 ± 0.048 (15) | 0.83 ± 0.056 (17) |

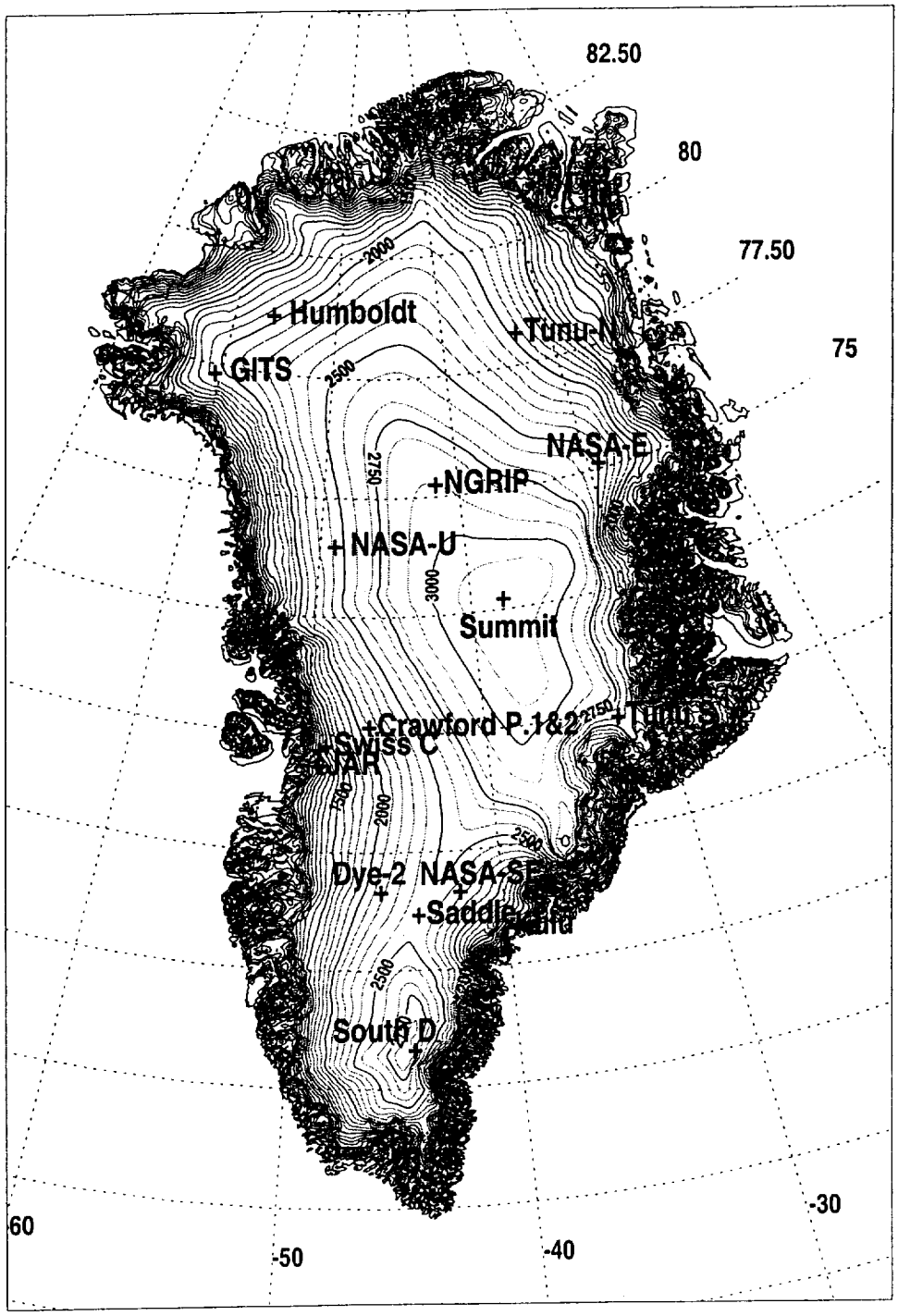
82.50
80
77.50
75
-30
-40
-50
60
+Humboldt
+GITS
+Tunu-N
NASA-E
+NGRIP
+NASA-U
Summit
+Crawford P.1&2
+Tunu-S
+Swiss C
+JAR
Dye-2
NASA-SE
+Saddle
South D
2000
2500
3000

Figure 1

AVHRR Polar Pathfinder Albedo Processing Steps

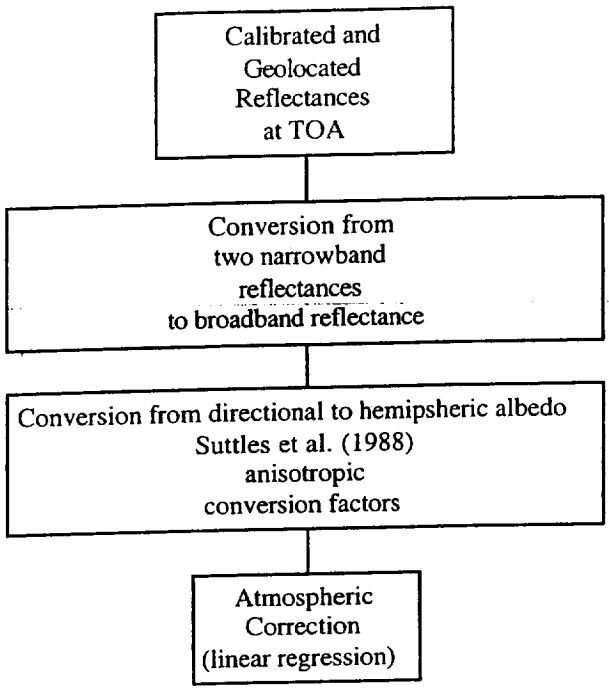


Figure 2

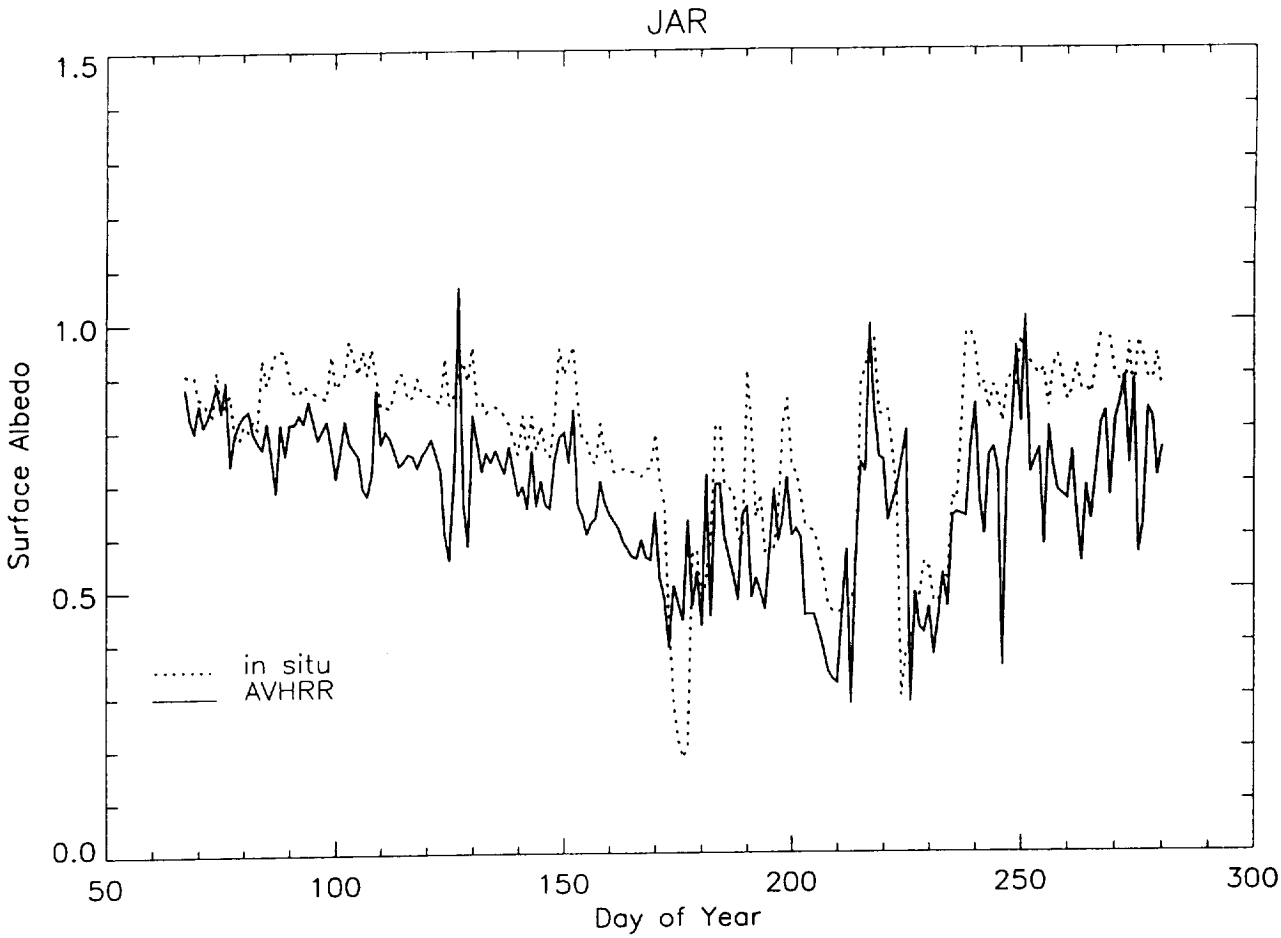
JAR
1.5
1.0
0.5
0.0
Surface Albedo
in situ
AVHRR
50
100
150
200
250
300
Day of Year

Figure 3(a)

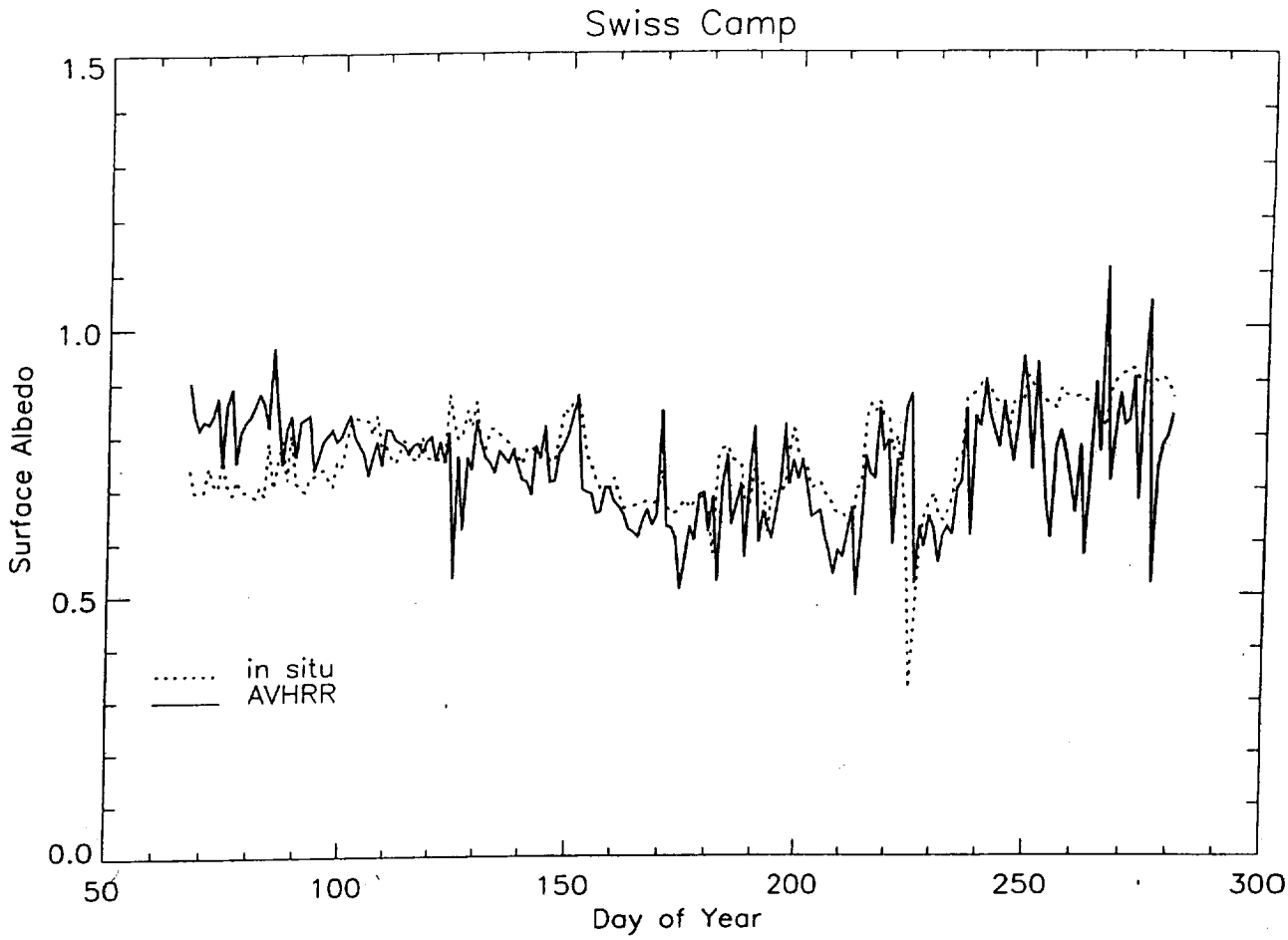
Swiss Camp
1.5
1.0
0.5
0.0
Surface Albedo
in situ
AVHRR
50
100
150
200
250
300
Day of Year

Figure 2(b)

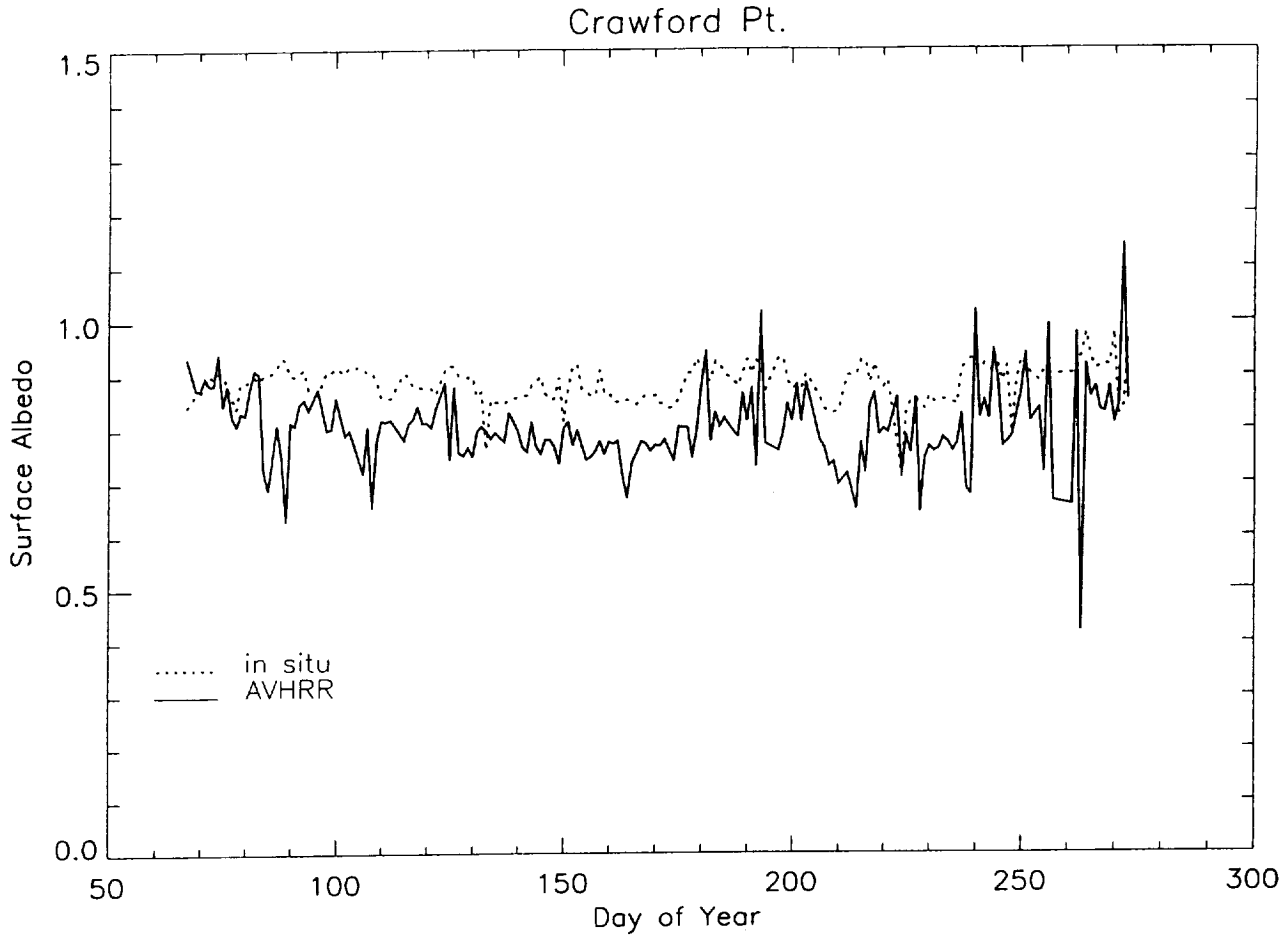
Crawford Pt.
1.5
1.0
0.5
0.0
Surface Albedo
in situ
AVHRR
50
100
150
200
250
300
Day of Year

Figure 3(c)

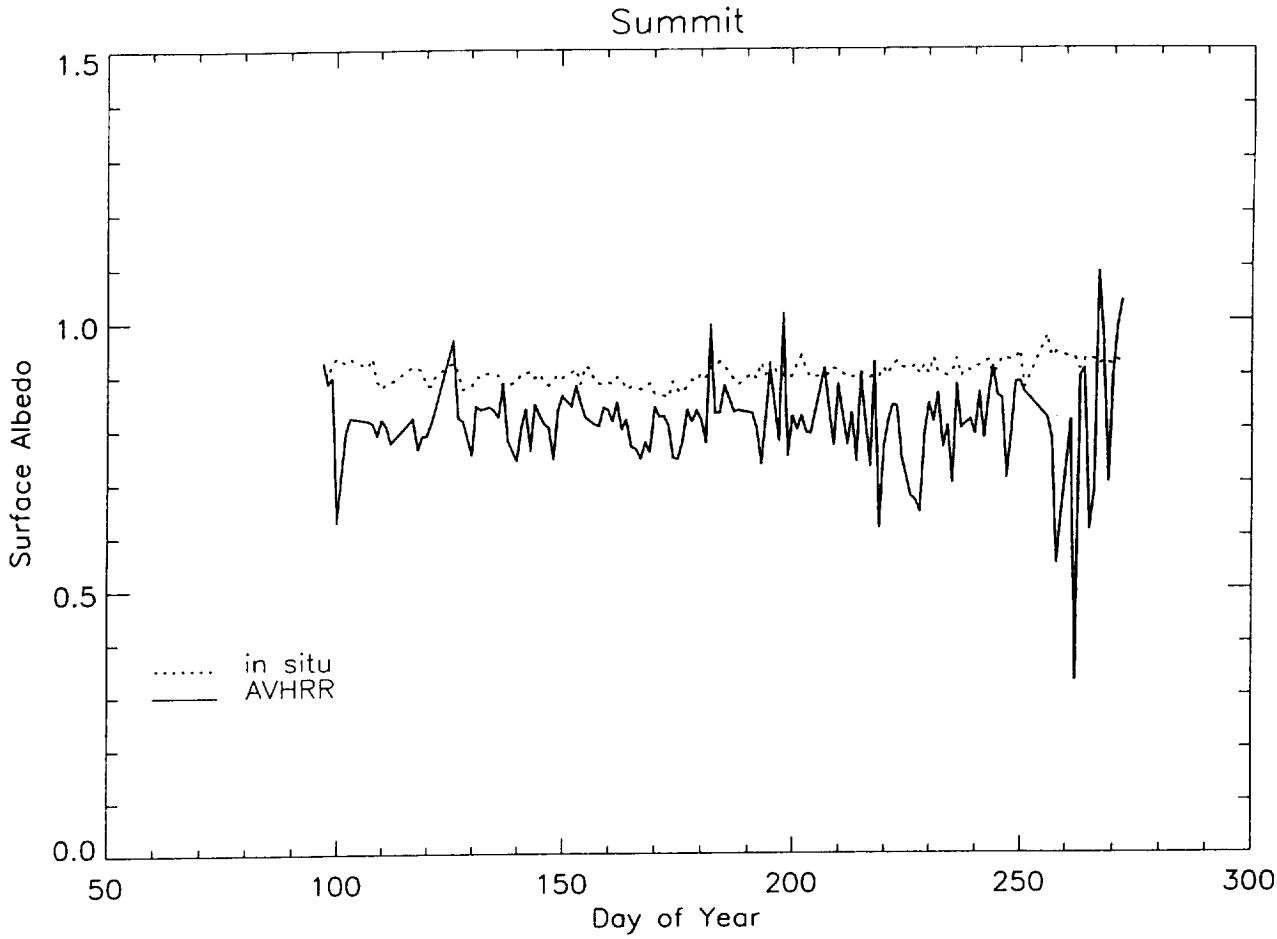
Summit
1.5
1.0
0.5
0.0
Surface Albedo
in situ
AVHRR
50
100
150
200
250
300
Day of Year

Figure 3(d)

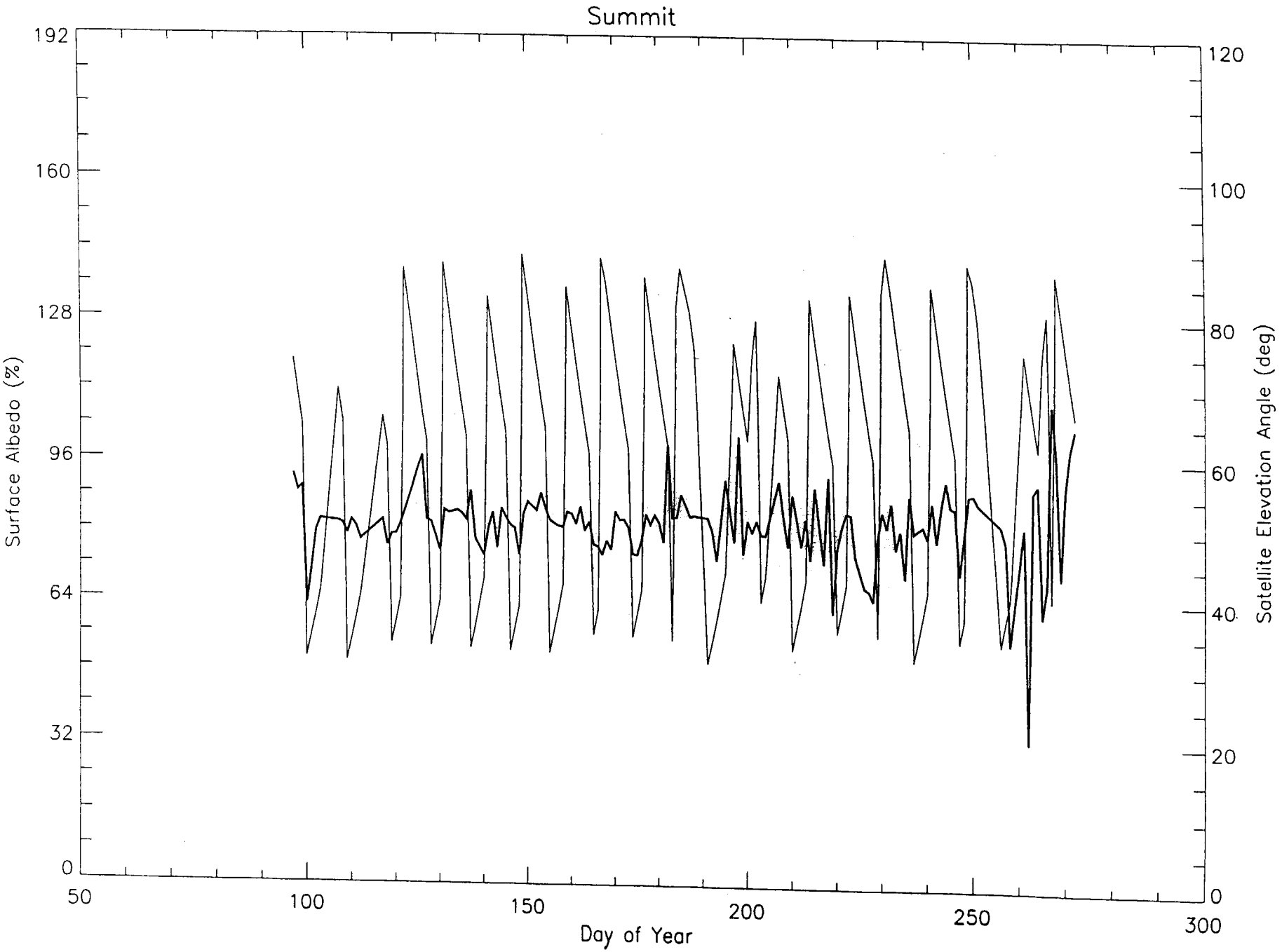
Summit
Surface Albedo (%)
192
160
128
96
64
32
0
Satellite Elevation Angle (deg)
120
100
80
60
40
20
0
50
100
150
200
250
300
Day of Year

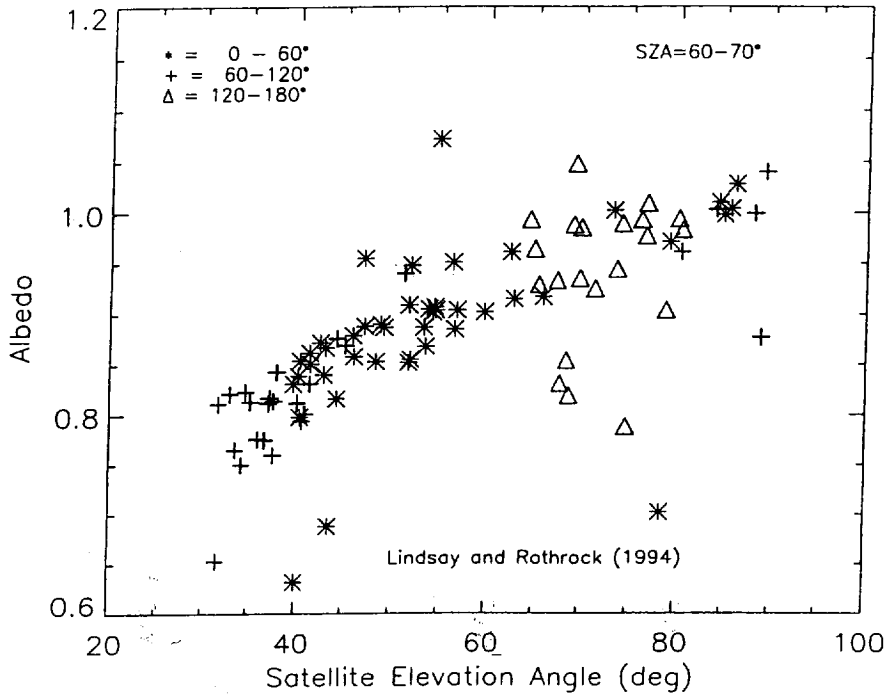
1.2
1.0
0.8
0.6
Albedo
* = 0 - 60°
+ = 60-120°
Δ = 120-180°
SZA=60-70°
Lindsay and Rothrock (1994)
20
40
60
80
100
Satellite Elevation Angle (deg)

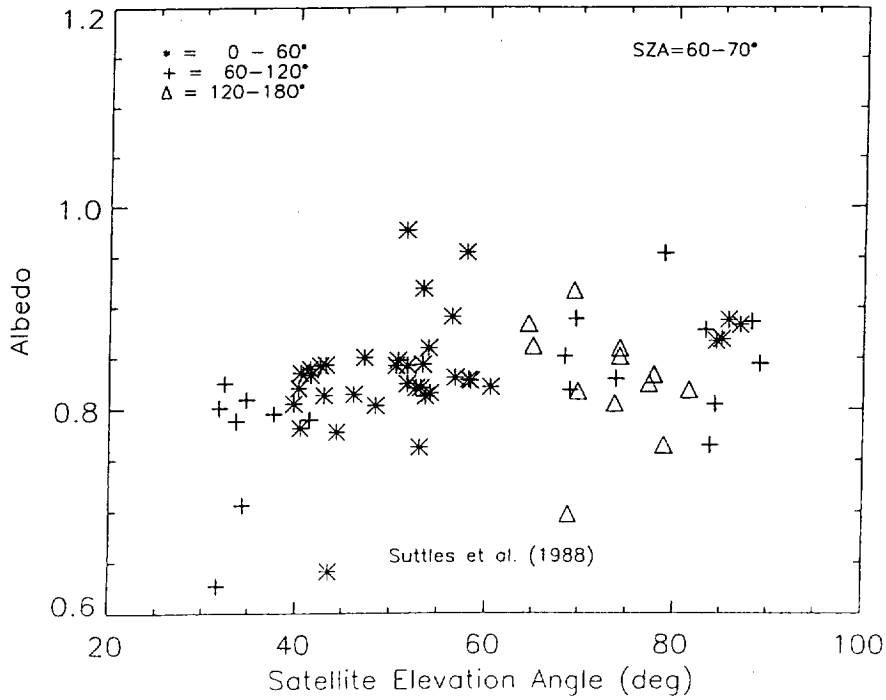
1.2
1.0
0.8
0.6
Albedo
* = 0 - 60°
+ = 60-120°
Δ = 120-180°
SZA=60-70°
Suttles et al. (1988)
20
40
60
80
100
Satellite Elevation Angle (deg)

Figure 5

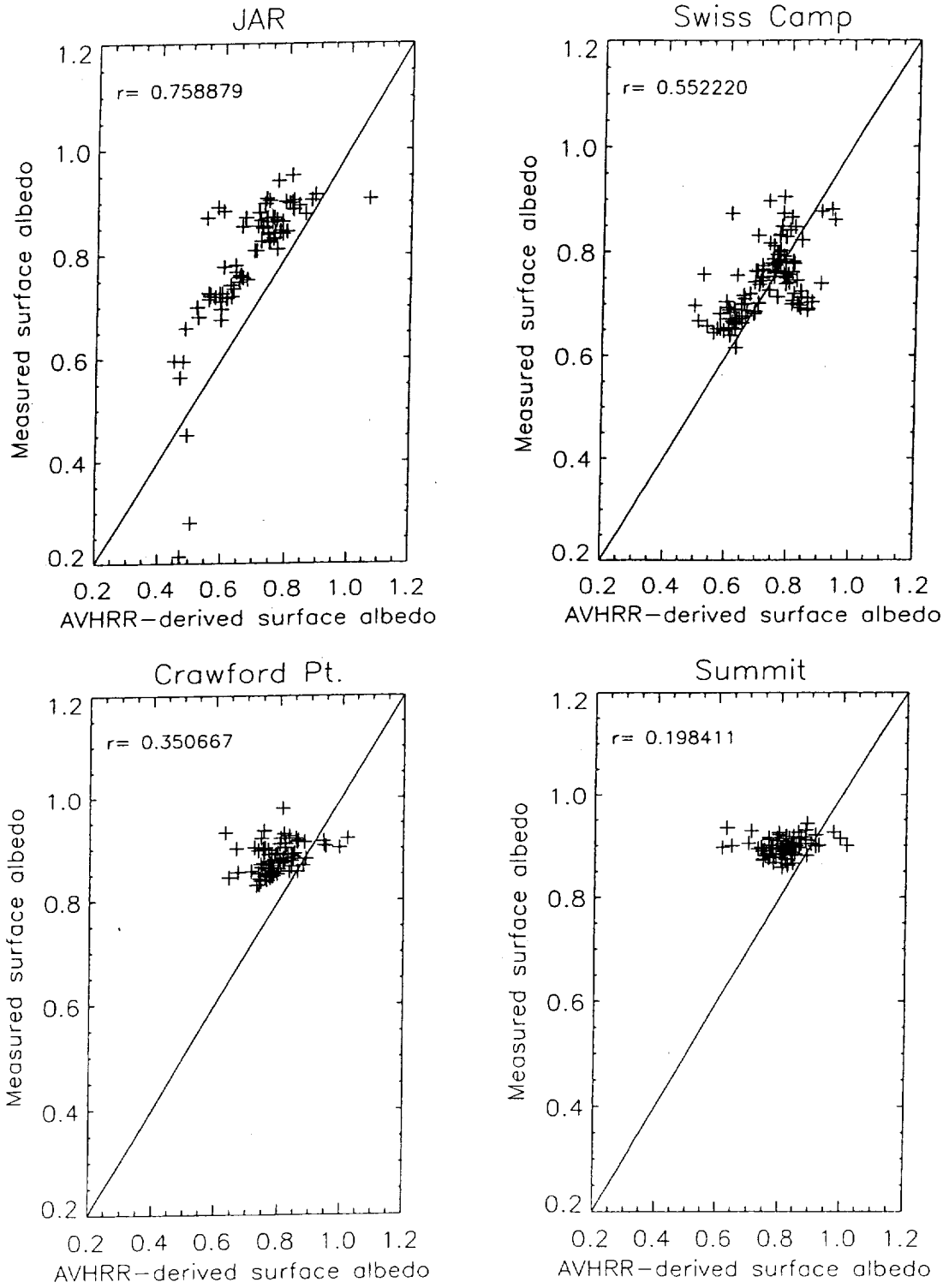
JAR
r= 0.758879
Measured surface albedo
AVHRR–derived surface albedo
Swiss Camp
r= 0.552220
Measured surface albedo
AVHRR–derived surface albedo
Crawford Pt.
r= 0.350667
Measured surface albedo
AVHRR–derived surface albedo
Summit
r= 0.198411
Measured surface albedo
AVHRR–derived surface albedo
0.2
0.4
0.6
0.8
1.0
1.2

Figure 6

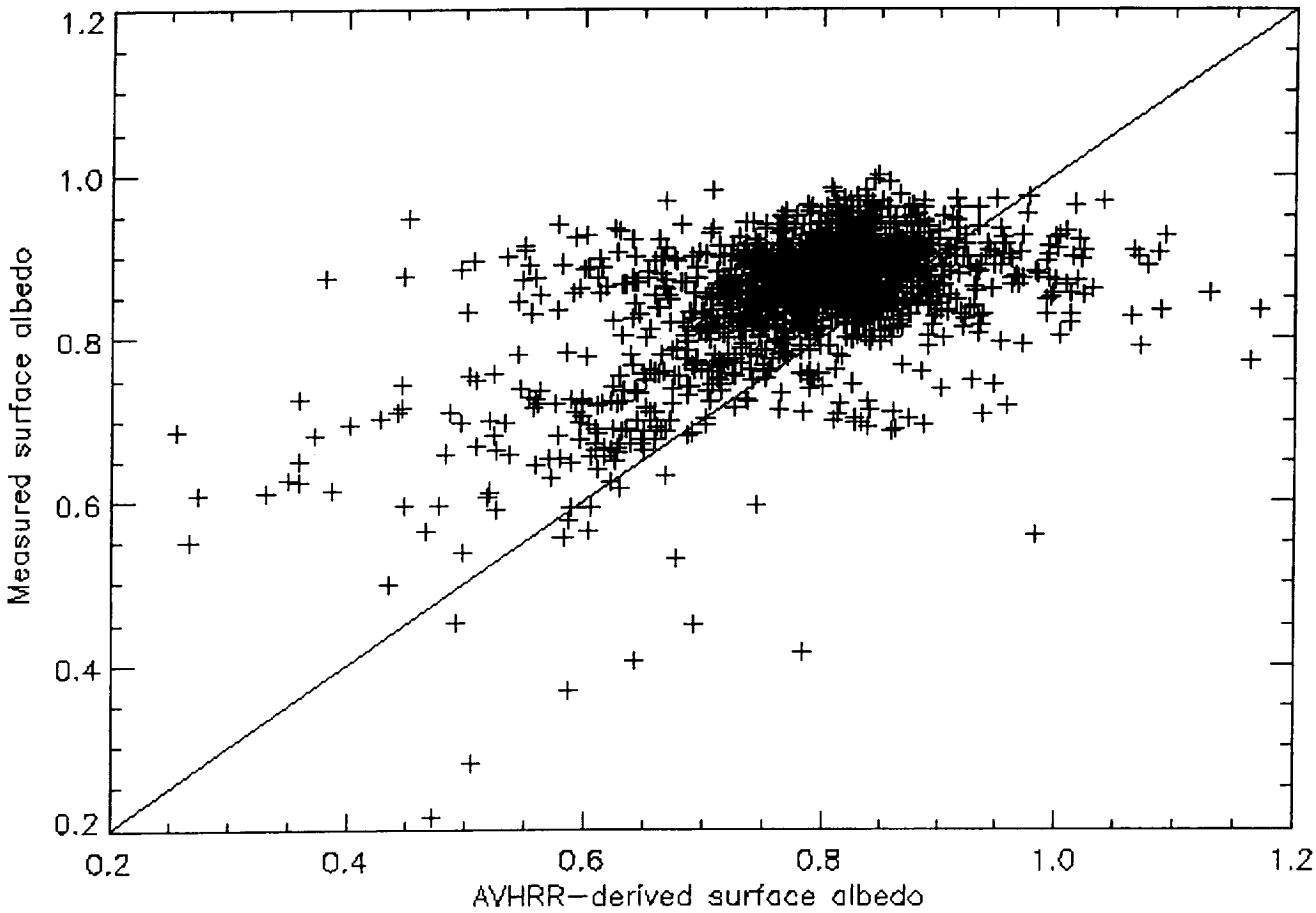
1.2
1.0
0.8
0.6
0.4
0.2
Measured surface albedo
0.2
0.4
0.6
0.8
1.0
1.2
AVHRR-derived surface albedo

Figure 7

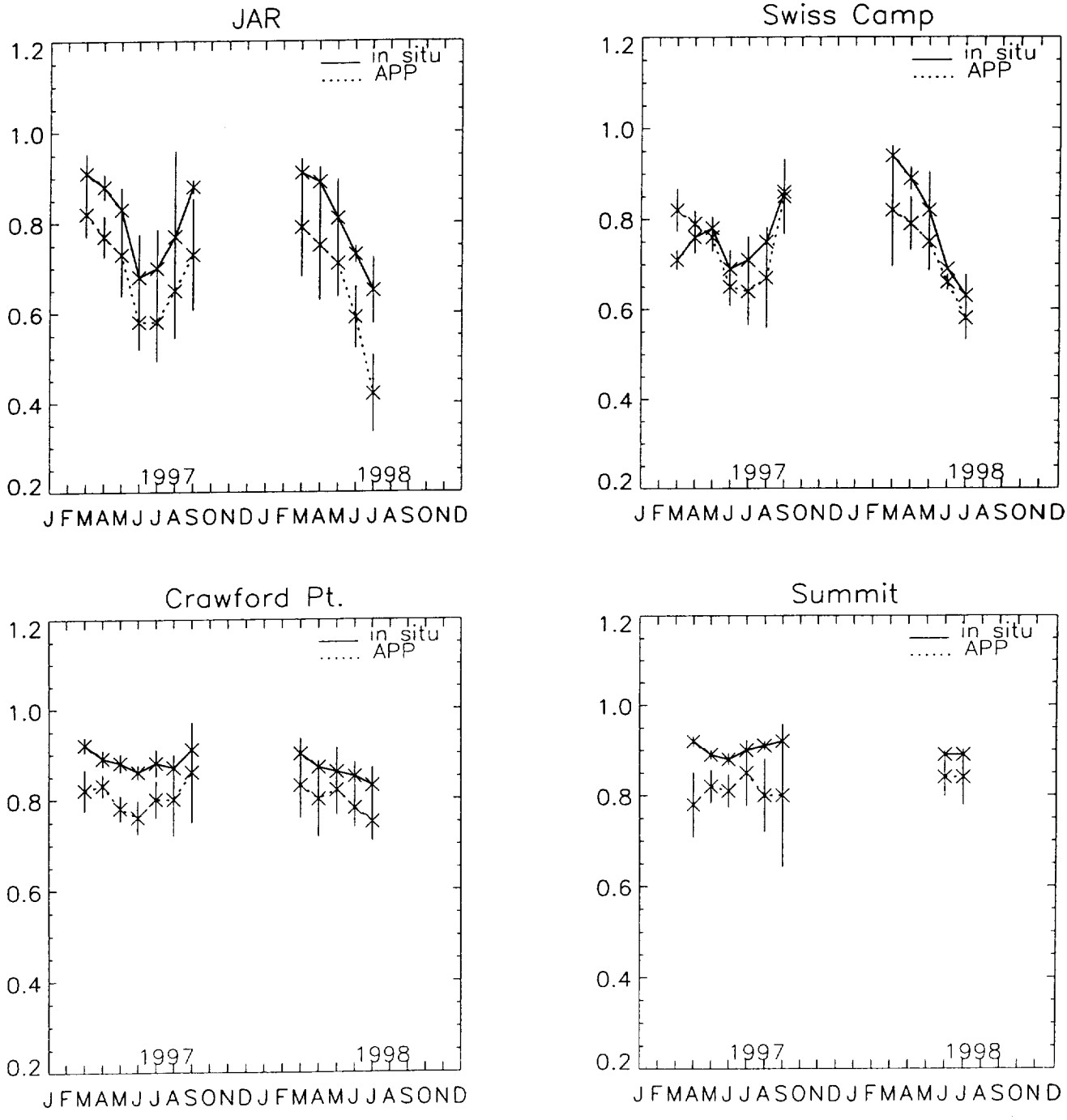
JAR
Swiss Camp
Crawford Pt.
Summit
in situ
APP
1.2
1.0
0.8
0.6
0.4
0.2
1997
1998
J F M A M J J A S O N D J F M A M J J A S O N D

Figure 8

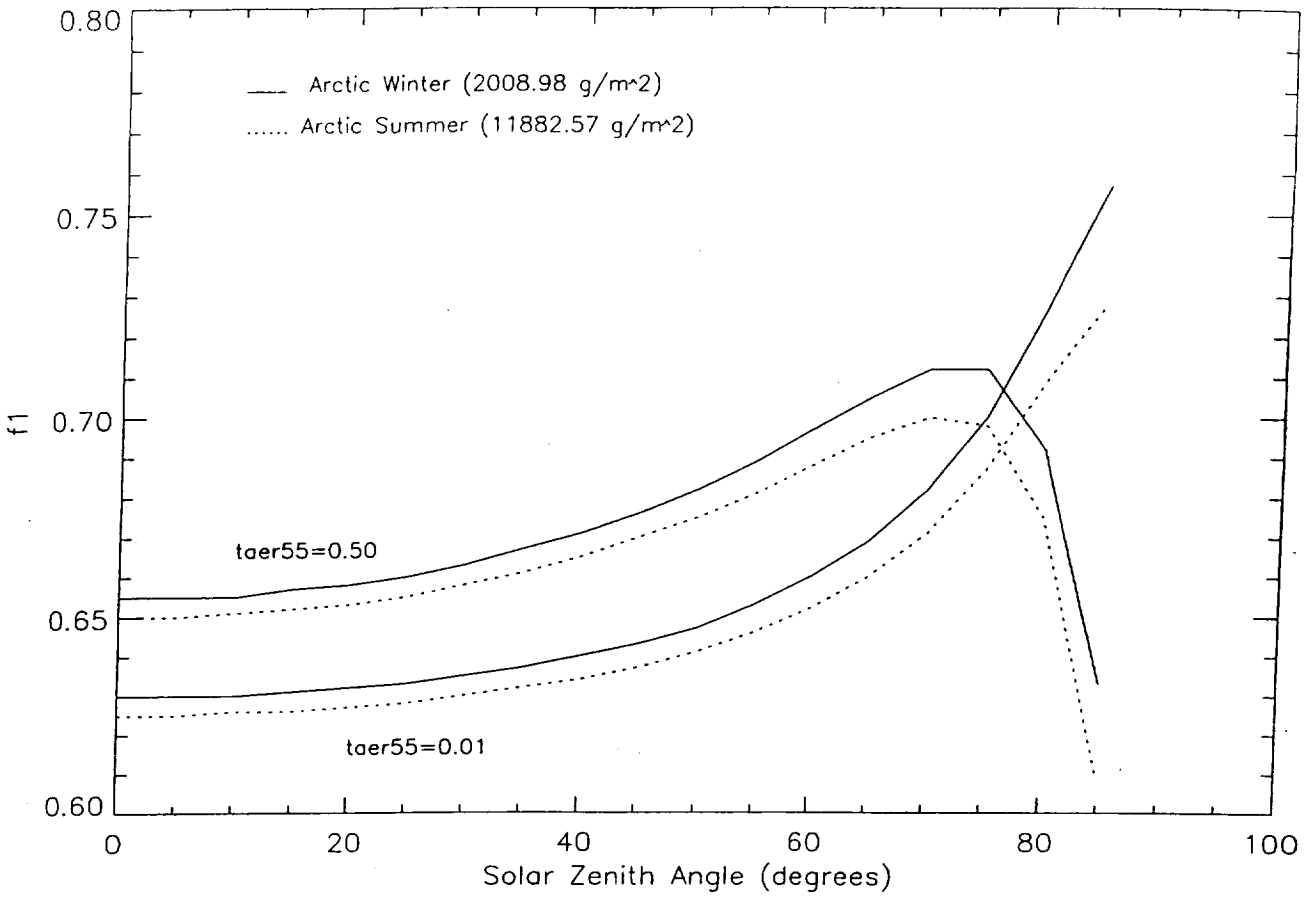
Arctic Winter (2008.98 g/m^2)
Arctic Summer (11882.57 g/m^2)
taer55=0.50
taer55=0.01
f1
0.80
0.75
0.70
0.65
0.60
0
20
40
60
80
100
Solar Zenith Angle (degrees)

Figure 9(a)

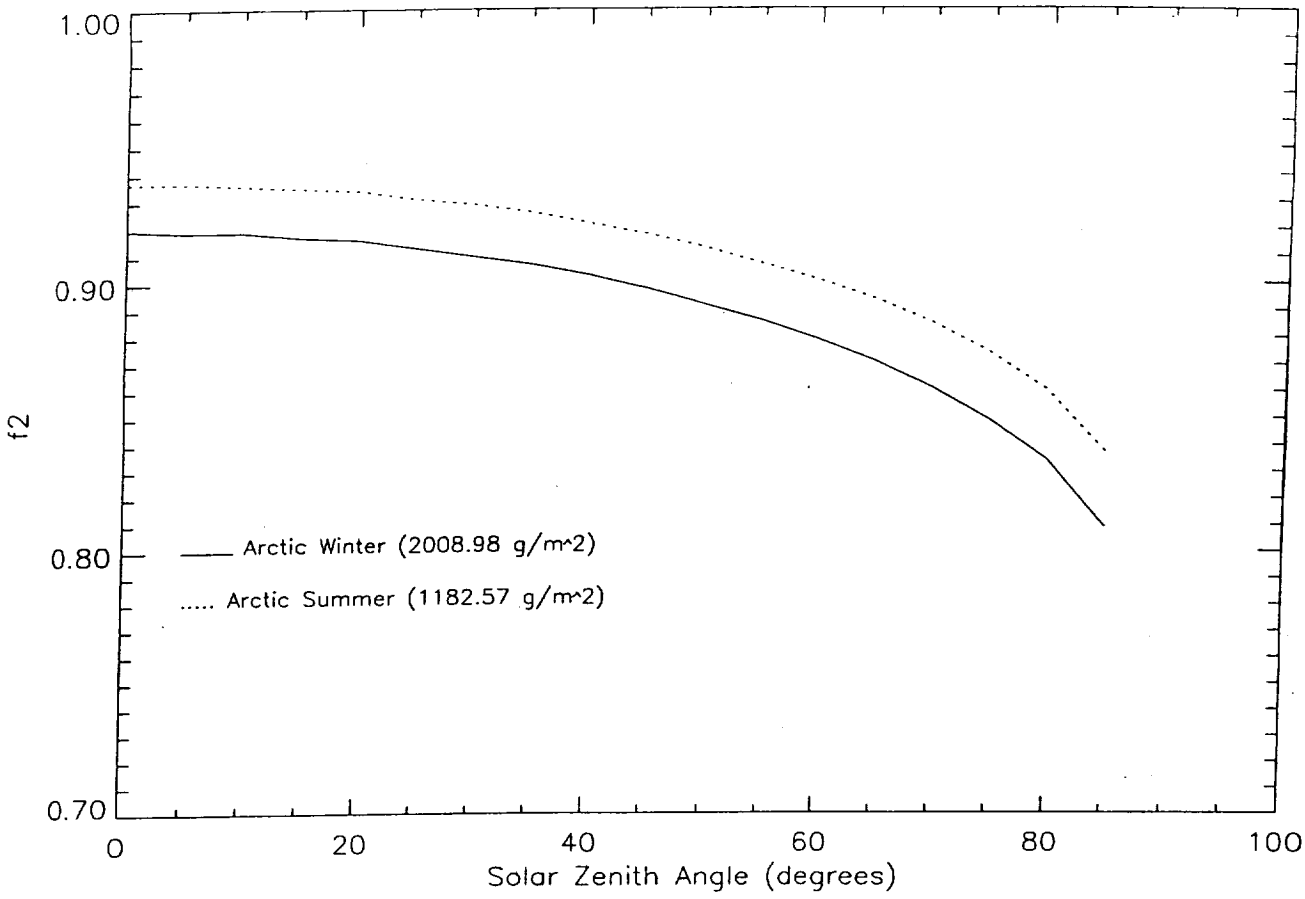
1.00
0.90
0.80
0.70
f2
Arctic Winter (2008.98 g/m^2)
Arctic Summer (1182.57 g/m^2)
0
20
40
60
80
100
Solar Zenith Angle (degrees)

Figure 9(b)

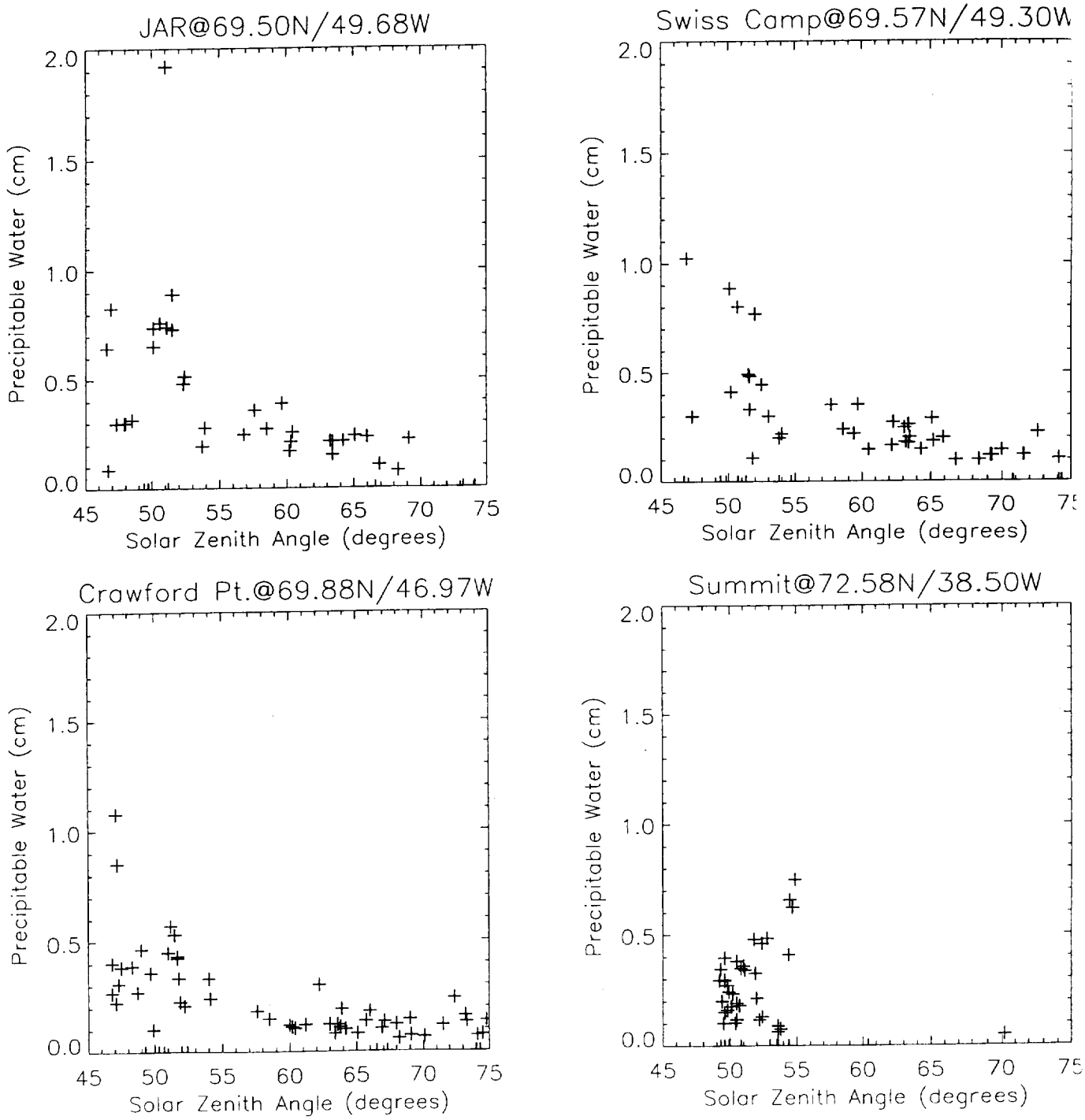
JAR@69.50N/49.68W
Swiss Camp@69.57N/49.30W
Crawford Pt.@69.88N/46.97W
Summit@72.58N/38.50W
Precipitable Water (cm)
Solar Zenith Angle (degrees)
0.0
0.5
1.0
1.5
2.0
45
50
55
60
65
70
75

Figure 10